

Joint 3D inversion of gravity and MT data using Gramian constraints: a case study from Yellowstone

Michael Jorgensen*, The University of Utah; and Michael S. Zhdanov, The University of Utah and TechnoImaging

Summary

The joint inversion of multiple geophysical datasets can produce more reliable models than the inversion of a single dataset; however, the implementation of the joint inversion can be challenging. There are two main approaches — the petrophysical approach and the structural approach. We detail both approaches based on a simultaneous joint inversion algorithm using the integral equation method coupled with a regularized conjugate gradient inversion. The development presented here is based on the use of Gramian constraints in a joint parametric functional to enforce structural similarity between jointly inverted density and resistivity models using either a direct correlation of the model parameters or a correlation of the gradients of the models. We demonstrate the effectiveness of the developed method and algorithm with two synthetic model studies and a case study of the joint inversion of gravity and magnetotelluric (MT) data acquired over Yellowstone National Park.

Introduction

In geophysical practice, multiple types of data are commonly gathered in exploratory surveys. As pertains to modeling and inversion, it can be more economical and efficient to conduct simultaneous joint inversions as opposed to separate inversions correlated after the fact. Joint inversion also has the added benefit of potentially limiting nonuniqueness in the models, which can simplify interpretation.

There are two main approaches to the joint inversion of geophysical data: the petrophysical approach and the structural approach. In the petrophysical approach, direct correlation is assumed to exist between the two modeled geophysical properties. For example, Sun and Li (2016) developed a deterministic joint inversion algorithm which seeks to improve a linear or nonlinear correlation between models by incorporating a priori petrophysical information. They inverted geophysical data in the spatial domain using petrophysical information through guided fuzzy c-means clustering in the parameter domain. This approach is, of course, dependent on the validity of the a priori petrophysical relationship. Haber and Oldenburg (1997) developed a generalized framework for a structural approach which would not be dependent on the direct correlation between the modeled parameters, but would enforce structural similarity between the models based on the correlation of a model property such as the gradient,

Laplacian, etc. An applied example of the structural approach would be the cross-gradients method of Gallardo (2007). It is based on the correlation of the gradients of the model parameters. Zhdanov et al. (2012) introduced a unified approach to joint inversion using Gramian constraints. In this generalized approach, it can be shown that methods based on direct correlations and/or structural constraints are special case reductions. Zhdanov et al. (2016) applied this approach to airborne electromagnetic and potential field data. This paper presents an application of the Gramian approach to the joint inversion of the gravity and MT data.

The workflow of the interpretation consists of performing separate 3D inversions of the gravity and MT data for selecting the model weighting and a priori model information. This is passed as input to the joint 3D inversion using Gramian constraints. The results of both separate and joint inversions are presented for two synthetic model studies to illustrate the effectiveness of the developed method and algorithm. We also consider a case study of the joint inversion of gravity and MT data acquired over Yellowstone National Park.

Forward modeling

We consider the g_z component of gravity field:

$$g_z(\mathbf{r}') = \gamma \iiint_D \rho(\mathbf{r}) \frac{z-z'}{|\mathbf{r}-\mathbf{r}'|^3} dv, \quad (1)$$

and the principal components of the impedance tensor, Z_{xy} and Z_{yx} , where the anomalous fields used to determine the impedance values are calculated using the following equations (Zhdanov and Keller, 1992):

$$\mathbf{E}^a(\mathbf{r}_j) = \iiint_D \widehat{\mathbf{G}}_E(\mathbf{r}_j|\mathbf{r}) \Delta\sigma(\mathbf{r}) (\mathbf{E}^b(\mathbf{r}) + \mathbf{E}^a(\mathbf{r})) dv, \quad (2)$$

$$\mathbf{H}^a(\mathbf{r}_j) = \iiint_D \widehat{\mathbf{G}}_H(\mathbf{r}_j|\mathbf{r}) \Delta\sigma(\mathbf{r}) (\mathbf{E}^b(\mathbf{r}) + \mathbf{E}^a(\mathbf{r})) dv, \quad (3)$$

and the integral equation method of Hursan and Zhdanov (2002).

Inversion

The gravity and MT inverse problems can be written in the form of the following operator equations:

Joint inversion using Gramian constraints

$$\mathbf{d}^{(i)} = A^{(i)} \mathbf{m}^{(i)}, (i = 1,2); \quad (4)$$

where $\mathbf{d}^{(i)}$ ($i = 1,2$) are the observed gravity and MT data, and $\mathbf{m}^{(i)}$ ($i = 1,2$) are the unknown density and geoelectrical resistivity distributions, respectively. Following the principles of Tikhonov regularization (Tikhonov and Arsenin, 1977) and Gramian stabilization (Zhdanov, 2015), we solve equations (4) by minimizing the following joint parametric functional:

$$P^\alpha(\mathbf{m}^{(1)}, \mathbf{m}^{(2)}) = \sum_{i=1}^2 \varphi^{(i)}(\mathbf{m}^{(i)}) + \sum_{i=1}^2 \alpha^{(i)} s_{MN}(\mathbf{m}^{(i)}) + \beta s_G(L^{(1)}\mathbf{m}^{(1)}, L^{(2)}\mathbf{m}^{(2)}), \quad (5)$$

where the terms $\varphi^{(i)}$ are the data misfit functionals:

$$\varphi^{(i)}(\mathbf{m}^{(i)}) = \|W_d^{(i)}(A^{(i)}(\mathbf{m}^{(i)}) - \mathbf{d}^{(i)})\|^2, (i = 1,2); \quad (6)$$

$W_d^{(i)}$ ($i = 1,2$) are the data weighting operators; and $A^{(i)}$ ($i = 1,2$) are the forward modeling operators. The terms $s_{MN}(\mathbf{m}^{(i)})$ are the minimum norm stabilizing functionals:

$$s_{MN}(\mathbf{m}^{(i)}) = \|W_m^{(i)}(\mathbf{m}^{(i)} - \mathbf{m}_{apr}^{(i)})\|^2, \quad (7)$$

where $W_m^{(i)}$ ($i = 1,2$) are the model weighting operators, and $\mathbf{m}_{apr}^{(i)}$ ($i = 1,2$) are the a priori models. The Gramian constraint term for a direct correlation of the model parameters, $s_G(L^{(1)}\mathbf{m}^{(1)}, L^{(2)}\mathbf{m}^{(2)})$, is defined as follows:

$$s_G(L^{(1)}\mathbf{m}^{(1)}, L^{(2)}\mathbf{m}^{(2)}) = \begin{vmatrix} (L^{(1)}\mathbf{m}^{(1)}, L^{(1)}\mathbf{m}^{(1)}) & (L^{(1)}\mathbf{m}^{(1)}, L^{(2)}\mathbf{m}^{(2)}) \\ (L^{(2)}\mathbf{m}^{(2)}, L^{(1)}\mathbf{m}^{(1)}) & (L^{(2)}\mathbf{m}^{(2)}, L^{(2)}\mathbf{m}^{(2)}) \end{vmatrix}, \quad (8)$$

where $L^{(i)}$ represents a linear transform of the model parameters, and the operation $(*,*)$ denotes the inner product of two vectors in the Gramian space. The linear transform allows us to map different model grids onto a common grid, and allows for nonlinear correlation of model parameters. We can also use the spatial derivatives of the model in the Gramian term, i.e., the gradient, the Laplacian, etc. This may be more appropriate for regions with complex geometry, where petrophysical correlations may not exist. In this structural approach, the Gramian term becomes:

$$s_G(\nabla \mathbf{m}^{(1)}, \nabla \mathbf{m}^{(2)}) = \begin{vmatrix} (\nabla \mathbf{m}^{(1)}, \nabla \mathbf{m}^{(1)}) & (\nabla \mathbf{m}^{(1)}, \nabla \mathbf{m}^{(2)}) \\ (\nabla \mathbf{m}^{(2)}, \nabla \mathbf{m}^{(1)}) & (\nabla \mathbf{m}^{(2)}, \nabla \mathbf{m}^{(2)}) \end{vmatrix}. \quad (9)$$

Finally, the terms $\alpha^{(i)}$ ($i = 1,2$) and β are adaptive regularization parameters which keep the stabilizers in check. The first iteration is run with these parameters set to zero, or no regularization. After the first iteration, the initial values are determined,

$$\alpha_0^{(i)} = \frac{\varphi^{(i)}(\mathbf{m}^{(i)})}{s_{MN}(\mathbf{m}^{(i)})}, \beta_0 = \frac{\varphi^{(i)}(\mathbf{m}^{(i)})}{s_G(L^{(1)}\mathbf{m}^{(1)}, L^{(2)}\mathbf{m}^{(2)})}, \quad (10)$$

and regularization on subsequent iterations is determined by the following progression of numbers:

$$\alpha_n^{(i)} = \alpha_0^{(i)} q^n, \beta_n = \beta_0 q^n, q < 1, \quad (11)$$

where n is the iteration number. The terms $\alpha^{(i)}$ ($i = 1,2$) and β are only decreased if the data misfit fails to decrease by a set threshold.

Data are normalized by the mean of the gravity data and the variance of the MT data, respectively; and scaled in the joint inversion such that the data misfits on the first iteration are unity. Model parameters are normalized by a function of the sensitivity and scaled in the joint inversion using information obtained in a separate datum inversion.

The parametric functional in (5) is minimized using the regularized conjugate gradient method outlined in Zhdanov (2015).

Three-layer box model study

It can be very difficult to resolve a low contrast anomaly directly overlying a high contrast anomaly in separately inverted density and resistivity models. We are able to resolve the layering of the model in Figure 1 using joint inversion with direct correlation of the model parameters. Conversely, in the separately inverted models, there is little geomorphological agreement and poor recovery of distinct layers. The data misfit for both separately and jointly inverted gravity models is $\sim 1\%$, and for the MT models $\sim 5\%$.

Joint inversion using Gramian constraints

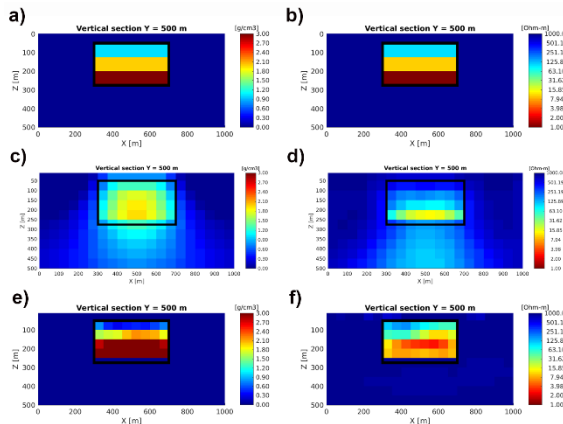


Figure 1: (a) True density model. (b) True resistivity model. (c) Separately inverted density model. (d) Separately inverted resistivity model. (e) Jointly inverted density model. (f) Jointly inverted resistivity model.

Yellowstone geologic setting

Huang et al. (2015) jointly inverted local and teleseismic P-wave data to develop the cartoon shown in Figure 2. They estimated the upper crustal rhyolitic partial melt reservoir volume to be roughly $10,000 \text{ km}^3$, and the lower crustal basaltic partial melt reservoir volume to be roughly $50,000 \text{ km}^3$. These low seismic velocity anomalies should correspond to the low density and high conductivity anomalies in our inversion results.

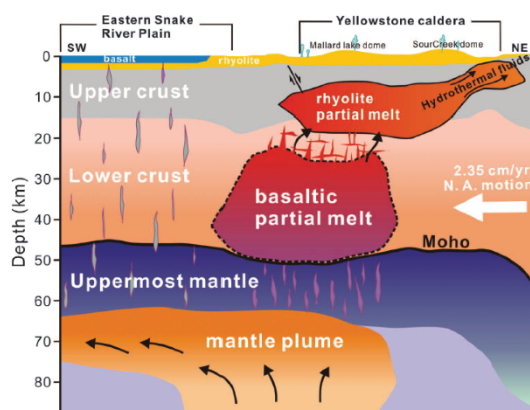


Figure 2: Cartoon of joint local and teleseismic P-wave inversion result from Huang et al. (2015). The chambers of rhyolite and basalt partial melt are used in the a priori models for the inversion.

Yellowstone model study (synthetic data)

Constructing models based on the seismic anomalies in Figure 2, we use the actual receiver components and locations used in the case study (shown in Figure 3) to

produce the inverted models shown in Figure 4. The joint inversion using a correlation of the gradients of the models successfully recovers two distinct bodies with significantly limited diffusivity. The data misfit for both separately and jointly inverted gravity models is $\sim 1\%$, and for the MT models $\sim 8\%$.

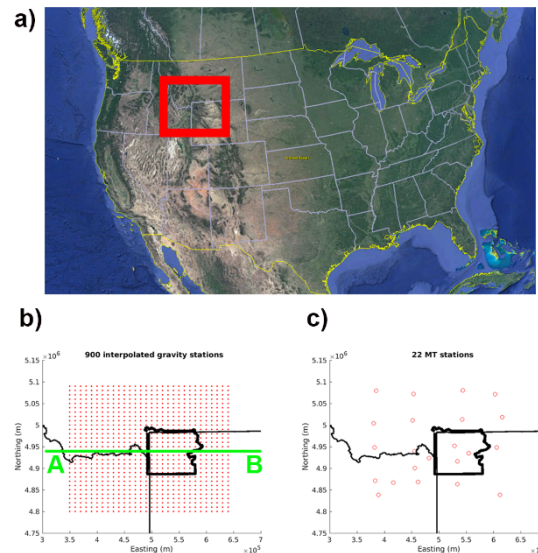


Figure 3: (a) Inversion domain shown in red is $400 \times 400 \times 80 \text{ km}$. (b) Gravity receiver locations. Line AB in green shows the location of the vertical sections. (c) MT receiver locations.

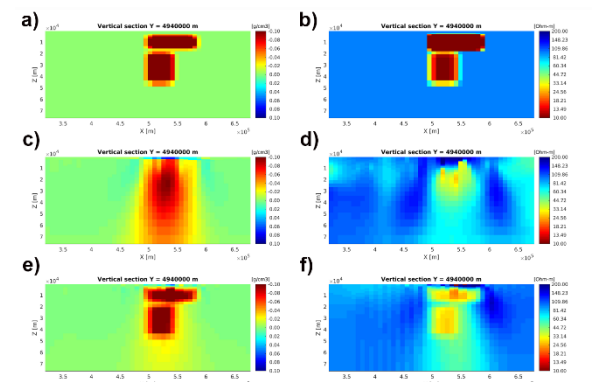


Figure 4: (a) True density model. (b) True resistivity model. (c) Separately inverted density model. (d) Separately inverted resistivity model. (e) Jointly inverted density model. (f) Jointly inverted resistivity model.

Yellowstone case study (real data)

We applied the developed method to gravity and MT data gathered around Yellowstone. Gravity data were downloaded from PACES (Webring, 2005), and MT data

Joint inversion using Gramian constraints

were collected as part of the Earthscope/USArray project. Gravity data (shown in Figure 5) were interpolated onto a common grid, Fourier transformed, and bandpass filtered to eliminate effects from the overlying sedimentary basin and deep mantle. Wavelengths 40-500 km were passed, which should correspond to a depth of investigation of roughly 1/6 or 6-83 km (Hinze et al., 2013).

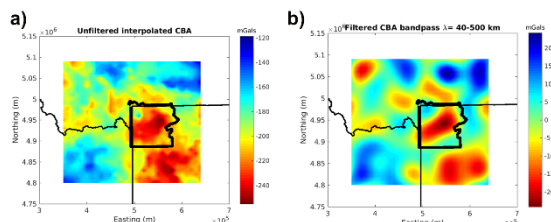


Figure 5: (a) Unfiltered complete Bouguer anomaly. (b) Bandpass filtered complete Bouguer anomaly.

A significant static shift was found in the MT data, and was removed using the complex distortion tensor method of Gribenko and Zhdanov (2015, 2017). Eight frequencies spanning 0.001-0.04 Hz were used. Model cells are 7.75 km to a side, with 36 logarithmically spaced vertical layers. The joint inversion was run from both homogeneous background and using a priori models based on the geomorphology of the true models in Figure 4, but with a very small contrast (5 Ohm-m and 0.01 g/cm³). Inverted models are shown in Figure 6. The data misfit for both separately and jointly inverted gravity models is ~1%, and for the MT models ~15%. We attribute this higher MT data misfit to sparse station coverage and a lack of higher frequencies in the data.

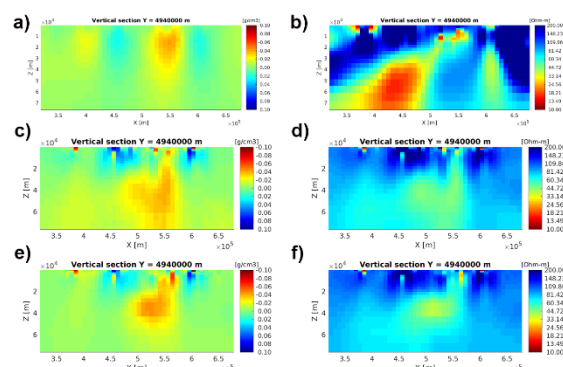


Figure 6: (a) Separately inverted density model. (b) Separately inverted resistivity model. (c) Jointly inverted density model without an a priori model. (d) Jointly inverted resistivity model without an a priori model. (e) Jointly inverted density model using an a priori model. (f) Jointly inverted resistivity model using an a priori model.

The separately inverted density and resistivity models are dissimilar. Both resolve the upper crustal rhyolitic chamber

of partial melt at depth of 5-15 km; however, they substantially deviate with respect to the lower crustal chamber of basaltic partial melt. A plume-like feature is recovered in the separately inverted resistivity model, which we do not see in the separately inverted density model. Conversely, the jointly inverted models show good geomorphological agreement. The lower crustal chamber of basaltic partial melt is recovered with a rough volume of 70,000 km³, and the upper crustal chamber of rhyolitic partial melt is recovered with a rough volume of 13,000 km³. These volumes, as well as the location of the anomalies recovered in the jointly inverted models, agree reasonably well with the jointly inverted seismic model referenced above.

Conclusions

We have applied a method of joint inversion based on the Gramian constraints to the interpretation of gravity and MT data. Our implementation is based on the integral equation method for computing gravity and MT data and Fréchet derivatives, and on the regularized conjugate gradient method for minimization of the joint parametric functional.

The synthetic model studies presented demonstrate that the jointly inverted models tend to more accurately represent the geomorphology of the region versus the separately inverted models, while still maintaining the same level of the data misfit and a good agreement between the observed and predicted fields. We have applied the developed method to data collected around the Yellowstone volcanic region. The recovered density and resistivity anomalies agree reasonably well with the results of joint local and teleseismic P-wave inversion for the same region.

Acknowledgements

The authors acknowledge the University of Utah's Consortium for Electromagnetic Modeling and Inversion (CEMI) for support of this research.

The MT data used in the inversion were acquired by the Incorporated Research Institutions for Seismology (IRIS) as part of the operation of the USArray. Data used in this study were made available through EarthScope (www.earthscope.org; EAR-0323309), supported by the National Science Foundation.

REFERENCES

- Gallardo, L. A., 2007, Multiple cross-gradient joint inversion for geospectral imaging: *Geophysical Research Letters*, **34**, L19301, <https://doi.org/10.1029/2007GL030409>.
- Gribenko, A. V., and M. S. Zhdanov, 2015, 3D inversion of regional MT data distorted by near-surface inhomogeneities using a complex distortion matrix: 85th Annual International Meeting, SEG, Expanded Abstracts, 984–989, <https://doi.org/10.1190/segam2015-5821800.1>.
- Gribenko, A. V., and M. S. Zhdanov, 2017, 3-D inversion of the MT Earth-Scope data, collected over the East Central United States: *Geophysical Research Letters*, **44**, 11800–11807, <https://doi.org/10.1002/2017GL075000>.
- Haber, E., and D. Oldenburg, 1997, Joint inversion: A structural approach: *Inverse Problems*, **13**, 63–67, <https://doi.org/10.1088/0266-5611/13/1/006>.
- Hinze, W. J., R. R. B. Von Frese, and A. H. Saad, 2013, Gravity and magnetic exploration: Cambridge University Press.
- Huang, H., F. Lin, B. Schmandt, J. Farrell, R. B. Smith, and V. C. Tsai, 2015, The Yellowstone magmatic system from the mantle plume to the upper crust: *Science*, **348**, 773–776, <https://doi.org/10.1126/science.aaa5648>.
- Hursan, G., and M. S. Zhdanov, 2002, Contraction integral equation method in three-dimensional electromagnetic modeling: *Radio Science*, **37**, 1089, <https://doi.org/10.1029/2001RS002513>.
- Sun, J., and Y. Li, 2016, Joint inversion of multiple geophysical data using guided fuzzy c-means clustering: *Geophysics*, **81**, no. 3, ID37–ID57, <https://doi.org/10.1190/GEO2015-0457.1>.
- Tikhonov, A. N., and V. Y. Arsenin, 1977, Solution of ill-posed problems: V.H. Winston and Sons.
- Webring, M., 2005, Terrain corrected United States gravity database, <https://gis.utep.edu>, accessed 10 January 2015.
- Zhdanov, M. S., 2015, Inverse theory and applications in geophysics: Elsevier.
- Zhdanov, M. S., A. V. Gribenko, and G. Wilson, 2012, Generalized joint inversion of multimodal geophysical data using Gramian constraints: *Geophysical Research Letters*, **39**, 1–7, <https://doi.org/10.1029/2012GL051233>.
- Zhdanov, M. S., and G. Keller, 1992, The geoelectrical methods of geophysical exploration: Elsevier.
- Zhdanov, M. S., Y. Zhu, M. Endo, and Y. Kinakin, 2016, Novel approach to joint 3D inversion of EM and potential field data using Gramian constraints: *First Break*, **34**, 59–64.